Distributed Learning over a Wireless Network with FSK-Based Majority Vote

Alphan Şahin
Electrical Engineering Department
University of South Carolina
Columbia, SC, USA
Email: asahin@mailbox.sc.edu

Bryson Everette
Electrical Engineering Department
University of South Carolina
Columbia, SC, USA
Email: everetb@email.sc.edu

Safi Shams Muhtasimul Hoque
Electrical Engineering Department
University of South Carolina
Columbia, SC, USA
Email: shoque@email.sc.edu

Abstract—In this study, we propose an over-the-air computation (AirComp) scheme for federated edge learning (FEEL). The proposed scheme relies on the concept of distributed learning by majority vote (MV) with sign stochastic gradient descend (signSGD). As compared to the state-of-the-art solutions, with the proposed method, edge devices (EDs) transmit the signs of local stochastic gradients by activating one of two orthogonal resources, i.e., orthogonal frequency division multiplexing (OFDM) subcarriers, and the MVs at the edge server (ES) are obtained with non-coherent detectors by exploiting the energy accumulations on the subcarriers. Hence, the proposed scheme eliminates the need for channel state information (CSI) at the EDs and ES. By taking path loss, power control, cell size, and the probabilistic nature of the detected MVs in fading channel into account, we prove the convergence of the distributed learning for a non-convex function. Through simulations, we show that the proposed scheme can provide a high test accuracy in fading channels even when the time-synchronization and the power alignment at the ES are not ideal. We also provide insight into distributed learning for location-dependent data distribution for the MV-based schemes.

Index Terms—Distributed learning, federated edge learning, FSK, OFDM, over-the-air computation, PMEPR.

I. Introduction

Federated edge learning (FEEL) is an implementation of federated learning (FL) in a wireless network to train a model without moving the local data generated at the edge devices (EDs) to an edge server (ES) [1], [2]. With FEEL, a large number of model parameters (or gradients) needs to be communicated between many EDs and the ES through wireless channels. However, typical user multiplexing methods such as orthogonal frequency division multiple access (OFDMA) can be inefficient to address the spectrum congestion due to a large number of EDs [3]. To address this issue, one of the promising solutions is to perform the calculations needed for FEEL, e.g., averaging, with an over-the-air computation (AirComp) method that harnesses the signal-superposition property of the wireless-multiple access channel [4]–[6]. However, developing an AirComp scheme is not a trivial task due to the multipath channel, power misalignment, and time-synchronization errors in practice. Also, the channel state information (CSI) needs to be available at the EDs or the ES with state-of-the-art solutions. In this study, we propose an AirComp scheme to address these issues.

In the literature, various AirComp schemes are proposed for FEEL. In [7], analog modulation over orthogonal frequency division multiplexing (OFDM) is investigated for broadband analog aggregation (BAA). Particularly, it is proposed to modulate the OFDM subcarriers with the model parameters at the EDs. To overcome the impact of the multipath channel on the transmitted signals, the symbols on the OFDM subcarriers are multiplied with the inverse of the channel coefficients and the subcarriers that fade are excluded from the transmissions, which is known as *truncated-channel inversion (TCI)* in the literature. In [8], an additional time-varying precoder is applied along with TCI to facilitate the aggregation. In [9], it is proposed to sparsify the gradient estimates and project the resultant sparse vector into a low-dimensional vector to reduce the bandwidth. The compressed data is transmitted with BAA. In [10], one-bit broadband digital aggregation (OBDA) is proposed to facilitate the implementation of FEEL for a practical wireless system. In this method, considering distributed training by majority vote (MV) with the sign stochastic gradient descend (signSGD) [11], the EDs transmit quadrature phase-shift keying (QPSK) symbols over OFDM subcarriers along with TCI, where the real and imaginary parts of the QPSK symbols are formed by using the signs of the stochastic gradients, i.e., votes. At the ES, the signs of the real and imaginary components of the superposed received symbols on each subcarrier are calculated to obtain the MV for the sign of each gradient. However, the EDs still need the CSI for TCI as in BAA for AirComp. In [12] and [13], blind EDs are considered. However, it is assumed that the CSI for each ED is available at the ES. The impact of the channel on AirComp is mitigated through beamforming with a large number of antennas.

In this study, we investigate an AirComp method based on non-coherent detection to achieve FEEL without using CSI at the EDs and the ES. Inspired by the MV with signSGD [11], we use orthogonal resources, i.e., multiple subcarriers and/or OFDM symbols, to transmit the signs of local stochastic gradients. Hence, the votes from different EDs accumulate on the orthogonal resources non-coherently in fading channel with the proposed scheme. The ES then obtains the MV with an energy detector. Considering the randomness in the detected MVs due to the fading channel, path loss, and power control in

the cell, we prove the convergence of learning in the presence of the proposed scheme for a non-convex loss function. We demonstrate that the proposed approach is robust against time-synchronization errors and power misalignment at the ES. We also show that it can be used with well-known peak-to-mean envelope power ratio (PMEPR) reduction techniques as it does not utilize the amplitude and the phase to encode the sign of local stochastic gradients. Finally, we evaluate the scheme by considering independent and identically distributed (IID) data and non-IID data where the data distribution is a function of the locations of EDs.

Notation: The complex and real numbers are denoted by $\mathbb{C}$ and $\mathbb{R}$, respectively. $\mathbb{E}[\cdot]$ is the expectation of its argument. $\mathbb{I}[\cdot]$ is the indicator function and $\mathbb{P}[\cdot]$ is the probability of its argument. The sign function is denoted by $\text{sign}(\cdot)$ and results in 1, -1, or ± 1 at random for a positive, a negative, or a zero-valued argument, respectively.

II. SYSTEM MODEL

A. Scenario

Consider a wireless network with K EDs that are connected to an ES, where each ED and the ES are equipped with single antennas. We assume that the frequency synchronization in the network is done before the transmissions with a control mechanism as done in 3GPP Fourth Generation (4G) Long Term Evolution (LTE) and/or Fifth Generation (5G) New Radio (NR) with random-access channel (RACH) and/or physical uplink control channel (PUCCH) [14]. In this study, we consider the fact that the time synchronization among the EDs is not ideal, and the maximum difference between the time of arrivals of the EDs signals at the ES location is T_{sync} seconds and it is equal to the reciprocal to the signal bandwidth.

In this study, the power alignment at the ES can be imperfect and the level of misalignment is controlled with a power control mechanism. We assume that the signal-to-noise ratio (SNR) of an ED at the ES is $1/\sigma_{\text{n}}^2$ at the reference distance R_{ref}. We then set the received signal power of the kth ED at the ES as

$$P_k = \left(\frac{r_k}{R_{\text{ref}}} \right)^{-(\alpha - \beta)} , \qquad (1)$$

where r_k is the link distance between the kth ED and the ES, α is the path loss exponent, and $\beta \in [0, \alpha]$ is a coefficient that determines the amount of the path loss compensated. While $\beta = 0$ means that there is no power control in the network, $\beta = \alpha$ leads to a system with perfect power alignment at the ES. We define the effective path loss exponent α_{eff} as $\alpha_{\text{eff}} \triangleq \alpha - \beta$.

In this study, we assume that the EDs are deployed in a cell, where the cell radius is R_{max} meters and the minimum distance between the ES and the EDs is R_{min} meters for $R_{\text{min}} \geq R_{\text{ref}}$. It is worth emphasizing that we do not consider the impact of multiple cells (e.g., inter-cell interference) or a more complicated large-scale channel model (e.g., shadowing) on learning in this work as our goal is to provide insights into the impact of power misalignment and the path loss on distributed learning with a tractable analysis.

B. Signal Model

In this study, for AirComp, the EDs access the wireless channel on the same time-frequency resources *simultaneously* with S OFDM symbols consisting of M active subcarriers. We assume that the cyclic prefix (CP) duration is larger than T_{sync} and the maximum-excess delays of the channel between the ES and the EDs. Considering independent frequency-selective channels between the EDs and the ES, the superposed symbol on the lth subcarrier of the mth OFDM symbol at the ES for the nth communication round of FEEL can be written as

$$r_{l,m}^{(n)} = \sum_{k=1}^{K} \sqrt{P_k} h_{k,l,m}^{(n)} t_{k,l,m}^{(n)} + n_{l,m}^{(n)} , \qquad (2)$$

where $h_{k,l,m}^{(n)} \in \mathbb{C}$ is the channel coefficient between the ES and the kth ED, $t_{k,l,m}^{(n)} \in \mathbb{C}$ is the transmitted symbol from the kth ED, and $n_{l,m}^{(n)}$ is the symmetric additive white Gaussian noise (AWGN) with zero mean and the variance σ_{n}^2 on the lth subcarrier for $l \in \{0, 1, \ldots, M-1\}$ and $m \in \{0, 1, \ldots, S-1\}$.

We consider the fact that the time synchronization at the receiver may not be precise. To model this, we assume that the synchronization point where the discrete Fourier transform (DFT) starts can deviate by N_{err} samples within the CP window. Note that the uncertainty of the synchronization point within the CP window is often not an issue for traditional communications due to the channel estimation. However, it can cause a non-negligible impact on AirComp.

Let $x(t_{\text{time}}) \in \mathbb{C}$ be a baseband OFDM symbol in continuous time for $t_{\text{time}} \in [0, T_{\text{s}})$, where T_{s} is the OFDM symbol duration. We define the PMEPR of an OFDM symbol as $\max_{t_{\text{time}} \in [0, T_{\text{s}})} |x(t_{\text{time}})|^2 / P_{\text{tx}}$, where $P_{\text{tx}} = \mathbb{E}\left[|x(t_{\text{time}})|^2 \right]$ is the mean-envelope power.

C. Learning Model

Let $\mathcal{D}_k$ denote the local data containing labeled data samples at the kth ED as $\{(\mathbf{x}_\ell, y_\ell)\} \in \mathcal{D}_k$ for $k = 1, \ldots, K$, where $\mathbf{x}_\ell$ and y_ℓ are ℓth data sample and its associated label, respectively. The centralized learning problem can be expressed as

$$\mathbf{w}^* = \arg\min_{\mathbf{w}} F(\mathbf{w}) = \arg\min_{\mathbf{w}} \frac{1}{|\mathcal{D}|} \sum_{\forall (\mathbf{x}, y) \in \mathcal{D}} f(\mathbf{w}, \mathbf{x}, y) , \quad (3)$$

where $\mathcal{D} = \mathcal{D}_1 \cup \mathcal{D}_2 \cup \cdots \cup \mathcal{D}_K$ and $f(\mathbf{w}, \mathbf{x}, y)$ is the sample loss function that measures the labeling error for $(\mathbf{x}, y)$ for the parameters $\mathbf{w} = [w_1, \ldots, w_q]^{\text{T}} \in \mathbb{R}^q$, and q is the number of parameters. With full-batch gradient descend, a local optimum point can be obtained as

$$\mathbf{w}^{(n+1)} = \mathbf{w}^{(n)} - \eta \mathbf{g}^{(n)} , \qquad (4)$$

where η is the learning rate and

$$\mathbf{g}^{(n)} = \nabla F(\mathbf{w}^{(n)}) = \frac{1}{|\mathcal{D}|} \sum_{\forall (\mathbf{x}, y) \in \mathcal{D}} \nabla f(\mathbf{w}^{(n)}, \mathbf{x}, y) , \quad (5)$$

where ith element of the vector $\mathbf{g}^{(n)}$ is the gradient of $F(\mathbf{w}^{(n)})$ with respect to $w_i^{(n)}$.

In [11], in the context of parallel processing, distributed training by MV with signSGD is investigated to solve (3). In this method, for the nth communication round, the kth ED[1] first calculates the local stochastic gradient as

$$\tilde{\mathbf{g}}_k^{(n)} = \nabla F_k(\mathbf{w}^{(n)}) = \frac{1}{n_\mathrm{b}} \sum_{\forall (\mathbf{x}_\ell, y_\ell) \in \tilde{\mathcal{D}}_k} \nabla f(\mathbf{w}^{(n)}, \mathbf{x}_\ell, y_\ell) , \quad (6)$$

where $\tilde{\mathcal{D}}_k \subset \mathcal{D}_k$ is the selected data batch from the local data set and $n_\mathrm{b} = |\tilde{\mathcal{D}}_k|$ as the batch size. Instead of the actual values of local gradients, the EDs then send the signs of their local stochastic gradients, denoted as $\bar{\mathbf{g}}_k^{(n)}$ for $k = 1, \ldots, K$, to the ES, where the ith element of the vector $\bar{\mathbf{g}}_k^{(n)}$ is $\bar{g}_{k,i}^{(n)} \triangleq \mathrm{sign}(\tilde{g}_{k,i}^{(n)})$. The ES obtains the MV for the ith gradient as

$$v_i^{(n)} \triangleq \mathrm{sign}\left(\sum_{k=1}^{K} \bar{g}_{k,i}^{(n)}\right) . \quad (7)$$

Subsequently, the ES pushes $\mathbf{v}^{(n)} = [v_1^{(n)}, \ldots, v_q^{(n)}]^\mathrm{T}$ to the EDs and the models at the EDs are updated as

$$\mathbf{w}^{(n+1)} = \mathbf{w}^{(n)} - \eta \mathbf{v}^{(n)} . \quad (8)$$

This procedure is repeated consecutively until a predetermined convergence criterion is achieved.

For FEEL, the optimization problem can also be expressed as (3) in a scenario where the local data samples and their labels are not available at the ES and the link between an ED and the ES experiences independent frequency-selective fading channel. To solve (3) under these constraints, in this study, we adopt the same procedure summarized for the distributed training by the MV. With the motivations of eliminating the latency caused by orthogonal multiple access and enabling distributed training in *mobile* wireless networks, we propose a simple-but-effective AirComp scheme to detect the MV in fading channel without using CSI at the EDs and the ES.

III. FSK-BASED MAJORITY VOTE

A. Edge Device - Transmitter

With the proposed AirComp scheme, the EDs perform a low-complexity operation to transmit the signs of the gradients given in (6): Let f be a bijective function that maps $i \in \{1, 2, \ldots, q\}$ to the distinct pairs (m^+, l^+) and (m^-, l^-) for $m^+, m^- \in \{0, 1, \ldots, S-1\})$ and $l^+, l^- \in \{0, 1, \ldots, M-1\}$. Based on the value of $\bar{g}_{k,i}^{(n)}$, at the nth communication round, the kth ED calculates the symbol $t_{k,l^+,m^+}^{(n)}$ and $t_{k,l^-,m^-}^{(n)}$, $\forall i$, as

$$t_{k,l^+,m^+}^{(n)} = \begin{cases} \sqrt{E_\mathrm{s}} \times s_{k,i}^{(n)} & \bar{g}_{k,i}^{(n)} = 1, \\ 0, & \bar{g}_{k,i}^{(n)} = -1 \end{cases}, \quad (9)$$

and

$$t_{k,l^-,m^-}^{(n)} = \begin{cases} 0, & \bar{g}_{k,i}^{(n)} = 1 \\ \sqrt{E_\mathrm{s}} \times s_{k,i}^{(n)}, & \bar{g}_{k,i}^{(n)} = -1 \end{cases}, \quad (10)$$

respectively, where $E_\mathrm{s} = 2$ is a factor to normalize the symbol energy and $s_{k,i}^{(n)}$ is a randomization symbol on the unit circle. Therefore, to indicate the sign of a local stochastic gradient, our scheme dedicates two subcarriers with (9) and (10), as opposed to modulating the phase of a subcarrier as done in OBDA. Also, we do not use TCI to compensate the impact of multipath channel on transmitted symbols as our goal is to exploit the energy accumulation on two different subcarriers to detect the MV with a non-coherent detector.

As a special case of f, if $m^- = m^+$ and $l^- = l^+ + 1$ hold for all i, the adjacent subcarriers of m^+th OFDM symbol forms the options for a vote, which corresponds to frequency-shift keying (FSK) over OFDM subcarriers. In this case, the kth ED's vote for the ith gradient becomes independent from its choice since the adjacent subcarriers are likely to experience similar channel conditions, i.e., $h_{k,l^+}^{(n)} \approx h_{k,l^++1}^{(n)}$. We refer to the MV calculation with the proposed scheme under this specific mapping as FSK-based MV (FSK-MV) in this study.

After the calculations of $t_{k,l^+,m^+}^{(n)}$ and $t_{k,l^-,m^-}^{(n)}$ for all i and k, the EDs calculate the OFDM symbols and transmit them based on the discussions in Section II.

B. Edge Server - Receiver

The receiver at the ES observes the superposed symbols at all subcarriers as expressed in (2). By using the mapping function f, the superposed symbols for a given i can be shown as

$$r_{l^+,m^+}^{(n)} = \sqrt{E_\mathrm{s}} \sum_{\forall k, \bar{g}_{k,i}^{(n)}=1} \sqrt{P_k} h_{k,l^+,m^+}^{(n)} s_{k,i}^{(n)} + n_{l^+,m^+}^{(n)} , \quad (11)$$

and

$$r_{l^-,m^-}^{(n)} = \sqrt{E_\mathrm{s}} \sum_{\forall k, \bar{g}_{k,i}^{(n)}=-1} \sqrt{P_k} h_{k,l^-,m^-}^{(n)} s_{k,i}^{(n)} + n_{l^-,m^-}^{(n)}. \quad (12)$$

respectively. The receiver at the ES detects the MV for the ith gradient with an energy detector as

$$v_i^{(n)} = \mathrm{sign}\left(\Delta_i^{(n)}\right) , \quad (13)$$

where $\Delta_i^{(n)} \triangleq e_i^+ - e_i^-$ for $e_i^+ \triangleq |r_{l^+,m^+}^{(n)}|_2^2$ and $e_i^- \triangleq |r_{l^+,m^+}^{(n)}|_2^2$, $\forall i$. It is worth mentioning that we do not use any method to resolve the interference in (11) and (12) among the EDs as we are not interested in the sign of a local gradients. On the contrary, we exploit the interference for aggregation and compare the amount of energy on two different subcarriers to detect the MV in (13). The transmitter and receiver block diagrams are provided in Fig. 1, based on the aforementioned discussions.

The proposed scheme leads to a fundamentally different training strategy since it determines the correct MV in (7) *probabilistically* by comparing e_i^+ and e_i^-. To elaborate this, assume that the multipath channels between the ES and the

---

[1]We refer to the workers and parameter-server mentioned in [11] as EDs and ES, respectively, to describe distributed training by MV with signSGD.
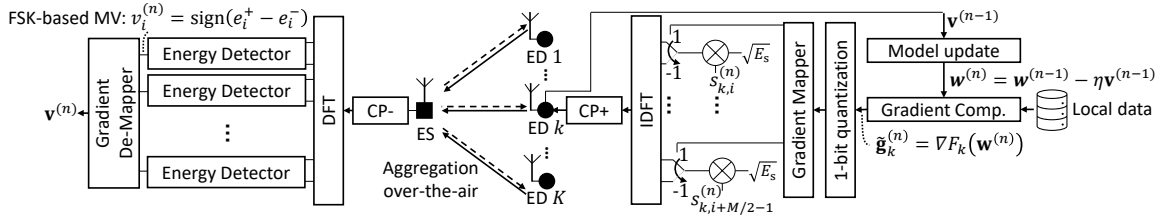
Fig. 1. Transmitter and receiver diagrams for implementing distributed learning over a wireless network with FSK-MV.

EDs are independent. Let K_i^+ and $K_i^- = K - K_i^+$ be the number of EDs that vote for 1 and -1 for the ith gradient, respectively.

Lemma 1. $\mathbb{E}\left[e_i^+\right]$ and $\mathbb{E}\left[e_i^-\right]$ can be calculated as

$$\mu_i^+ \triangleq \mathbb{E}\left[e_i^+\right] = E_s K_i^+ \lambda + \sigma_n^2 , \qquad (14)$$

and

$$\mu_i^- \triangleq \mathbb{E}\left[e_i^-\right] = E_s K_i^- \lambda + \sigma_n^2 , \qquad (15)$$

respectively, where

$$\lambda \triangleq \begin{cases} \dfrac{2R_{\text{ref}}^{\alpha_{\text{eff}}}}{R_{\max}^2 - R_{\min}^2} \dfrac{R_{\min}^{2-\alpha_{\text{eff}}} - R_{\max}^{2-\alpha_{\text{eff}}}}{\alpha_{\text{eff}} - 2} , & \alpha_{\text{eff}} \neq 2 \\ \dfrac{2R_{\text{ref}}^{\alpha_{\text{eff}}}}{R_{\max}^2 - R_{\min}^2} \ln \dfrac{R_{\max}}{R_{\min}} , & \alpha_{\text{eff}} = 2 \end{cases} . \qquad (16)$$

Proof: Since (11) is a weighted summation of independent complex Gaussian random variables with zero mean and unit variance (i.e., channel coefficients), $r_{l^+,m^+}^{(n)}$ is a zero mean random variable, where its variance is

$$\mu_i^+ = \mathbb{E}\left[e_i^+\right] = \mathbb{E}\left[|r_{l^+,m^+}^{(n)}|_2^2\right] = \mathbb{E}\left[E_s \sum_{\bar{g}_{\forall k,i}^{(n)}=1} \left(\frac{r_k}{R_{\text{ref}}}\right)^{-\alpha_{\text{eff}}} + \sigma_n^2\right]$$
$$= E_s K_i^+ \mathbb{E}\left[\left(\frac{r_k}{R_{\text{ref}}}\right)^{-\alpha_{\text{eff}}}\right] + \sigma_n^2 . \qquad (17)$$

To calculate (17), we need to calculate the expected value of $y = r^{-\alpha_{\text{eff}}}$. Assuming that the EDs are localized uniformly within the cell, the link distance distribution can be expressed as

$$f(r) = \frac{2r}{R_{\max}^2 - R_{\min}^2} . \qquad (18)$$

Hence, the distribution of y can obtained as

$$f(y) = \left.\frac{f(r)}{|\frac{dy}{dr}|}\right|_{r=y^{-\frac{1}{\alpha_{\text{eff}}}}} = \frac{2y^{-\frac{\alpha_{\text{eff}}+2}{\alpha_{\text{eff}}}}}{(R_{\max}^2 - R_{\min}^2)\alpha_{\text{eff}}} . \qquad (19)$$

By using (19), the expected value of y can be calculated as (16). The same analysis can be done for μ_i^-. ∎

Based on Lemma 1, (13) is likely to obtain the correct MV because μ_i^+ and μ_i^- are linear functions of K_i^+ and K_i^-, respectively. However, the detection performance depends on the parameter $\lambda \in [0,1]$ that captures the impacts of power control, path loss, and cell size on e_i^+ and e_i^-. In Fig. 2, we plot λ for different cell sizes for a given α_{eff}. For a better power

control or a smaller cell size, the parameter λ increases to 1, which implies a better detection performance under noise. On the other hand, the MV is not deterministic for $\sigma_n^2 = 0$. Hence, the convergence for a non-convex loss function $F(\mathbf{w})$ needs to be shown to justify if the proposed scheme is suitable for FEEL.

C. Convergence in Fading Channel

We consider several standard assumptions made in the literature for the convergence analysis [10], [11]:

Assumption 1 (Bounded loss function). $F(\mathbf{w}) \geq F^*, \forall \mathbf{w}$.

Assumption 2 (Smoothness). Let $\mathbf{g}$ be the gradient of $F(\mathbf{w})$ evaluated at $\mathbf{w}$. For all $\mathbf{w}$ and $\mathbf{w}'$, the expression given by

$$\left|F(\mathbf{w}') - (F(\mathbf{w}) - \mathbf{g}^T(\mathbf{w}' - \mathbf{w}))\right| \leq \frac{1}{2}\sum_{i=1}^{q} L_i(w_i' - w_i)^2 ,$$

holds for a non-negative constant vector $\mathbf{L} = [L_1,...,L_q]^T$.

Assumption 3 (Variance bound). The stochastic gradient estimates $\{\tilde{\mathbf{g}}_k = [\tilde{g}_{k,1},...,\tilde{g}_{k,q}]^T = \nabla F_k(\mathbf{w}^{(n)})\}, \forall k$, are independent and unbiased estimates of $\mathbf{g} = [g_1,...,g_q]^T = \nabla F(\mathbf{w})$ with a coordinate bounded variance, i.e.,

$$\mathbb{E}\left[\tilde{\mathbf{g}}_k\right] = \mathbf{g}, \ \forall k, \qquad (20)$$
$$\mathbb{E}\left[(\tilde{g}_{k,i} - g_i)^2\right] \leq \sigma_i^2/n_b, \ \forall k, i, \qquad (21)$$

where $\boldsymbol{\sigma} = [\sigma_1,...,\sigma_q]^T$ is a non-negative constant vector.

Assumption 4 (Unimodal, symmetric gradient noise). For any given $\mathbf{w}$, the elements of the vector $\tilde{\mathbf{g}}_k, \forall k$, has a unimodal distribution that is also symmetric around its mean.

We also assume that the parameters e_i^+ and e_i^- are exponential random variables, where their means are μ_i^+ and μ_i^-, respectively. This assumption holds true when the power control is ideal under IID Rayleigh fading. It is a weak assumption under imperfect power control due to the central limit theorem.

By extending our theorem in [15] with the considerations of path loss, power control, and cell size, the convergence rate in the presence of FSK-MV can obtained as follows:
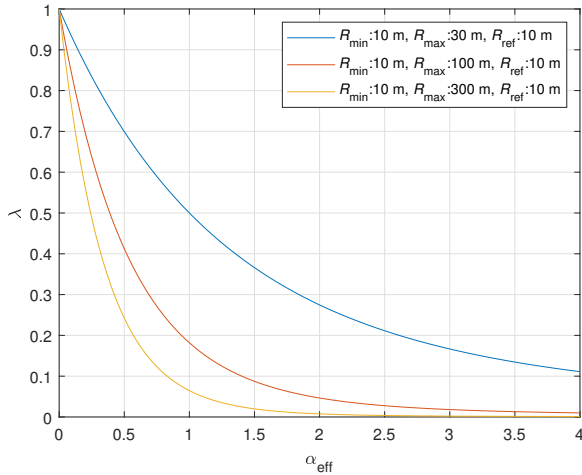
Fig. 2. Impact of cell size and the effective path loss exponent on λ.

Layer	Learnables
Input ($28 \times 28 \times 1$ images)	N/A
Convolution 2D (5×5, 20 filters)	Weights: $5 \times 5 \times 1 \times 20$ Bias: $1 \times 1 \times 20$
Batchnorm	Offset: $1 \times 1 \times 20$ Scale: $1 \times 1 \times 20$
ReLU	N/A
Convolution 2D (3×3, 20 filters)	Weights: $3 \times 3 \times 20 \times 20$ Bias: $1 \times 1 \times 20$
Batchnorm	Offset: $1 \times 1 \times 20$ Scale: $1 \times 1 \times 20$
ReLU	N/A
Convolution 2D (3×3, 20 filters)	Weights: $3 \times 3 \times 20 \times 20$ Bias: $1 \times 1 \times 20$
Batchnorm	Offset: $1 \times 1 \times 20$ Scale: $1 \times 1 \times 20$
ReLU	N/A
Fully-connected layer (10 outputs)	Weights: 10×11520 Bias: 10×1
Softmax	N/A

Theorem 1. For $n_b = N/\gamma$ and $\eta = 1/\sqrt{\|\mathbf{L}\|_1 n_b}$, the convergence rate of the distributed training by the MV based on FSK in fading channel is

$$\mathbb{E}\left[\frac{1}{N}\sum_{n=0}^{N-1}\|\mathbf{g}^{(n)}\|_1\right] \leq \frac{1}{\sqrt{N}}\left(a\sqrt{\|\mathbf{L}\|_1}\left(F(\mathbf{w}^{(0)}) - F^* + \frac{\gamma}{2}\right)\right.$$
$$\left. + \frac{2\sqrt{2}}{3}\sqrt{\gamma}\|\boldsymbol{\sigma}\|_1\right), \quad (22)$$

where γ is a positive integer, $a = (1 + \frac{2}{\xi K})\frac{1}{\sqrt{\gamma}}$ for $\xi \triangleq \frac{E_s\lambda}{\sigma_n^2}$, and $\lambda \in [0, 1]$ given in (16) is a parameter that captures the parameters related to the path loss, power control, and cell size.

The proof of Theorem 1 is given in the appendix.

Based on Theorem 1, we can infer the followings: 1) For a larger SNR (i.e., a larger $1/\sigma_n^2$) and a large number of EDs (i.e., a larger K), the convergence rate with FSK-MV in fading channel improves since a decreases. 2) The power control results in a better convergence rate since λ increases with a lower α_{eff}. 3) Another way of improving the convergence rate is to reduce to cell size, yielding a large λ as illustrated in Fig. 2. However, this indicates a practical limitation of a single-cell FEEL: The number of EDs may be smaller for a smaller cell. However, the power control becomes a harder task for a larger cell. 4) Finally, under ideal power control, the convergence rate becomes similar to the one with signSGD in an ideal channel [11, Theorem 1] asymptotically.

D. Comparisons

1) Robustness against Time-Varying Fading Channel: As opposed to the approaches in [7] and [10], the proposed scheme does not utilize the CSI for TCI at the EDs. Hence, it is compatible with time-varying channels (e.g., mobile networks [16]) and does not lose gradient information due to TCI. As a trade-off, it quadruples the number of time-frequency resources for AirComp as compared to OBDA in [10]. As compared to the approaches in [12] and [13], the proposed scheme also does not require CSI at the ES or multiple antennas.

2) Robustness against Time-Synchronization Errors: As demonstrated in Section IV, the proposed scheme provides immunity against the time-synchronization errors. This is because the timing misalignment among the EDs or the uncertainty on the receiver synchronization within the CP window cause phase rotations in the frequency domain and FSK-MV does not encode information on the amplitude or phase. Also, the proposed scheme does not use any channel-related information at the EDs and the ES. Hence, FSK-MV is more robust against time-synchronization errors as compared to OBDA.

3) Robustness against Power-Amplifier Non-linearity: The proposed scheme separates the options for voting over two different resources identified in time and frequency. Hence, it allows one to choose $s_{k,i}^{(n)}$ based on specific purposes. In this study, we use random QPSK symbol to reduce PMEPR by decreasing the correlation in the frequency domain [17]. OBDA is not investigated in terms of PMEPR in the literature. As shown in Section IV, OBDA can suffer from high PMEPR, while the proposed scheme reduces PMEPR with a simple randomization technique. Also, FSK-MV does not require a long transmission power constraint as in introduced for OBDA [10, Eq. 9 and Eq. 10] since the ℓ_2-norm of the OFDM symbols do not change as a function of CSI with FSK-MV.

IV. NUMERICAL RESULTS

For the numerical results, we consider the learning task of handwritten-digit recognition in a single cell with $K = 50$ EDs for $R_{\text{min}} = 10$ meters and $R_{\text{max}} = 100$ meters. We assume that the path loss exponent is $\alpha = 4$. To demonstrate the impact of the imperfect power control on distributed learning, we choose $\beta \in \{2, 4\}$ and set the SNR, i.e., $1/\sigma_n^2$, to be 20 dB at $R_{\text{ref}} = 10$ meters. The link distance between the kth ED and
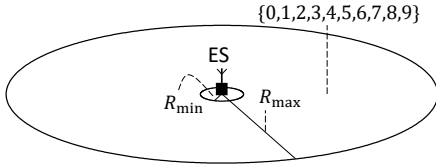
(a) IID data in the cell. All EDs have data samples for 10 different digits.
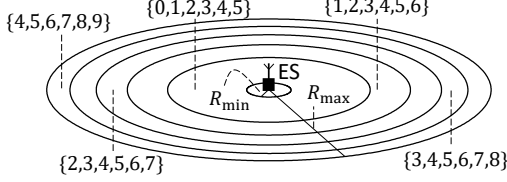
(b) Non-IID data in the cell. The available digits at the EDs change based on their locations in the cell. The digits in an area are shown in the figure.

Fig. 3. IID versus non-IID data considered for the numerical analyses. The radius of the concentric circles are $\{10, 45.6, 63.7, 77.7, 89.6, 100\}$ meters.

the ES is set to $r_k = \sqrt{R_{\text{min}}^2 + (k-1)(R_{\text{max}}^2 - R_{\text{min}}^2)/(K-1)}$ based on (18). For the fading channel, we consider ITU Extended Pedestrian A (EPA) with no mobility and regenerate the channels between the ES and the EDs independently for each communication round to capture the long-term channel variations. The subcarrier spacing is set to 15 kHz. We use $M = 1200$ subcarriers (i.e., the signal bandwidth is 18 MHz). In the case of imperfect time synchronization, we assume that the difference between time of arriving ED signals is maximum $T_{\text{sync}} = 55.6$ ns and the synchronization uncertainty at the ES is $N_{\text{err}} = 3$ samples. Otherwise, these parameters are set to 0.

For the local data at the EDs, we use the MNIST database that contains labeled handwritten-digit images size of 28×28 from digit 0 to digit 9[2]. We consider both IID data and non-IID data in the cell. To prepare the data, we first choose $|\mathcal{D}| = 25000$ training images from the database, where each digit has distinct 2500 images. For the scenario with the IID data, we assume that each ED has 50 distinct images for each digit. For the scenario with the non-IID data, we assume that the distribution of the images depends on the locations of the EDs to test the FEEL in a more challenging scenario. To this end, we divide the cell into 5 areas with concentric circles and the EDs located in uth area have the data samples with the labels $\{u-1, u, 1+u, 2+u, 3+u, 4+u\}$ for $u \in \{1, ..., 5\}$. Hence, the availability of the labels gradually changes based on the link distance. The areas between two adjacent concentric circles are identical and the number of EDs in each area is 10. The IID and non-IID data distributions are illustrated in Fig. 3.

For the model, we consider a convolution neural network (CNN) that includes one 5×5 and two 3×3 convolutional layers, where each of them is followed by a batch normalization layer and rectified-linear unit (ReLU) activation follow each of them. All convolutional layers have 20 filters. After

[2]For FEEL, the data samples are generated at the EDs. We distribute the data samples in the MNIST database to the EDs to generate representative results for FEEL.

the third ReLU, a fully-connected layer with 10 units and a softmax layer are utilized. At the input layer, no normalization is applied. Our model, outline in Table I, has $q = 123090$ learnable parameters, which corresponds to $S = 206$ and $S = 52$ OFDM symbols for the FSK-MV and OBDA [10], respectively. For TCI, the truncation threshold is 0.2 and we assume that CSI is available at the EDs. For the update rule, the learning rate is set to 0.01. The batch size n_{b} is set to 64. For the test accuracy calculations, we use 10000 test samples available in the MNIST database.

In Fig. 4, we provide the test accuracy results for IID/non-IID data in the cell by taking time-synchronization errors and imperfect power control. For the same configurations, we provide the local loss values at the EDs as function of link distance in Fig. 5 after $N = 500$ communication rounds. In Fig. 4(a) and Fig. 4(b), we consider the IID data in the cell. We evaluate the scenarios with the non-IID data in Fig. 4(c) and Fig. 4(d). For Fig. 4(a), the power alignment at the ES is assumed to be perfect (i.e., $\alpha_{\text{eff}} = 0$). The results in this figure indicate that OBDA works well when the time synchronization is ideal and the CSI is available at the EDs. However, OBDA without TCI or its utilization under imperfect time synchronization cause drastic reductions in the performance. On the other hand, the FSK-MV is robust against the time-synchronization errors and result a high test accuracy without using CSI at the EDs as it is based on non-coherent detection and dedicates two orthogonal resources to indicate the sign of the gradient. In Fig. 4(b)-(d), we observe the same trends for OBDA and FSK-MV. However, the maximum test accuracy is highly affected by the data distribution and the power control. In Fig. 4(b), the power alignment at the ES is not ideal (i.e., $\alpha_{\text{eff}} = 2$). Although the test accuracy with OBDA with TCI (with ideal synchronization) or FSK-MV (with/without ideal synchronization) reaches to 95%, Fig. 5(b) indicates the local losses increase at the EDs as compared to the ones in Fig. 5(a). In this scenario, the distributed learning exploits the IID-data in the cell, which also benefits to the cell-edge EDs that have the similar data distributions to the ones at the nearby EDs. In Fig. 4(c), we see the impact of the non-IID data on the test accuracy. Although the power alignment is ideal in this case, the maximum test accuracy reduces to 75% from 95%. We observe more degradation in accuracy in Fig. 4(d), where the power control is not ideal. In Fig. 5(c) and Fig. 5(d), we can identify the digits that are not learned well. In the case of ideal power control, based on Fig. 5(c), we observe that the digit 0 and the digit 9 are not learned well since these digits are available in less number of EDs as compared to other digits. Hence, the MV is highly biased. A similar issue arises when the power control is not perfect. As shown in Fig. 5(d), the local loss function tend to increase with the distance, i.e., the cell-edge EDs's data are not learned. As the cell-edge EDs' received signal powers are weak as compared the ones for the nearby EDs, the MV is again biased toward the nearby EDs local data. Therefore, the digits available at the cell-edge EDs, e.g., digits 6, 7, 8, and 9, are not learned well. Both issues in the case of non-IID data
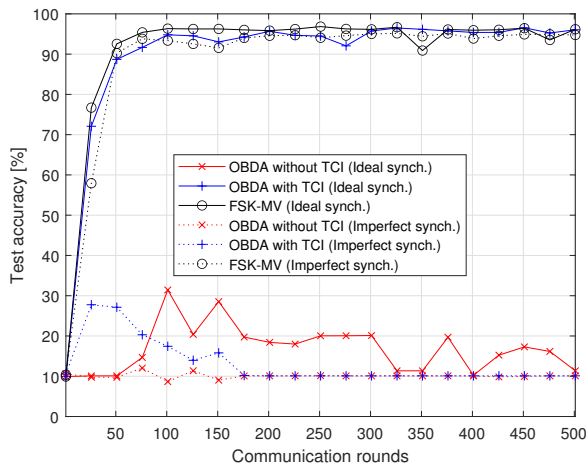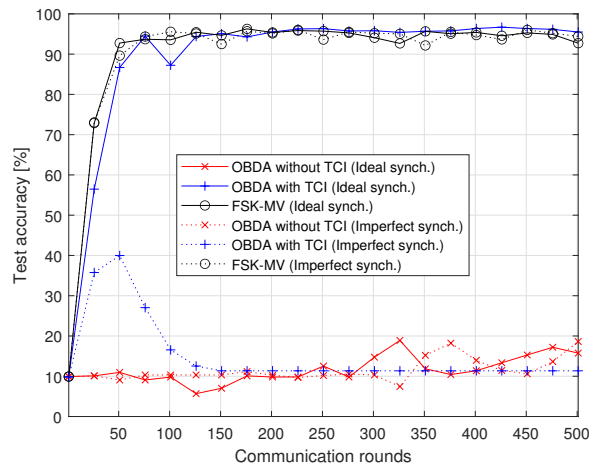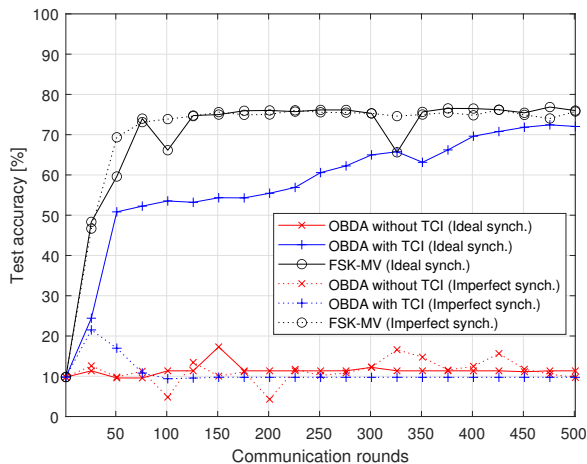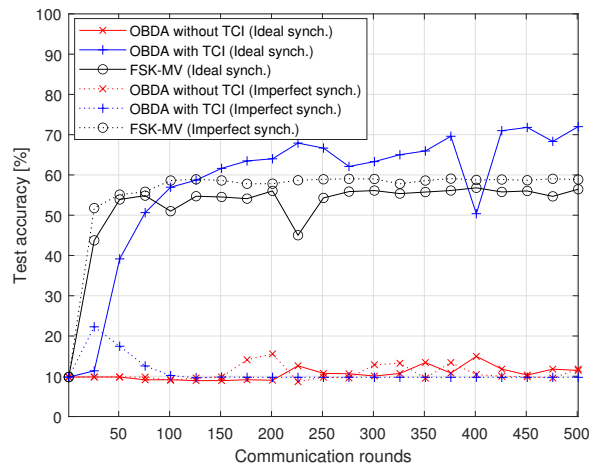
Fig. 4. Test accuracy versus communication rounds. FSK-MV works without the CSI at the EDs and ES and provide robustness against time-synchronization errors. The test accuracy reduces more for non-IID when the power control is imperfect.

indicate that an adaptive learning strategy that takes the bias in the MV into account (e.g., through an adaptive ED selection or a power control based on the label distribution) is needed for achieving a higher test accuracy.

Finally, we compare the PMEPR distributions in Fig. 6 for OBDA and FSK-MV. Since the proposed scheme introduces randomness in the frequency domain with the randomization symbols, it exhibits a similar behavior to a typical OFDM transmission in terms of PMEPR. On the other hand, the OBDA can cause substantially high PMEPR for OFDM as the signs of the gradients can be highly-correlated.

V. CONCLUDING REMARKS

In this study, we propose an effective AirComp scheme for FEEL. The proposed scheme relies on the distributed learning by the MV with the signSGD in fading channel. As compared to the state-of-the-art solutions on AirComp, it uses different subcarriers and/or OFDM symbols to indicate the sign of the local stochastic gradients. Thus, it allows the receiver at the ES to detect the MV with a non-coherent detector and eliminates the need for CSI at the EDs by exploiting the non-coherent

energy accumulation on the subcarriers. We also prove the convergence of the distributed learning by taking path loss, power control, and cell size into account. Through simulations, we demonstrate that the proposed method can provide a high test accuracy in fading channel even when the power control and the time synchronization are imperfect while resulting in an acceptable PMEPR distribution at the expense of a larger number of time and frequency resources. We also provide insights into the scenarios where local data distribution depends on the locations of the EDs and demonstrate the impact of non-IID data on the distributed learning when the power control is not ideal. Our results indicate that adaptive learning methods that consider the bias in the MV due to the non-IID data and/or imperfect power control are required for achieving a higher test accuracy.

APPENDIX
PROOF OF THEOREM 1

Proof: The proof of Theorem 1 relies on a well-known strategy of relating the norm of the gradient of the loss function $F(\mathbf{w})$ to the expected improvement made in a single step as

(a) IID data, ideal power control ($\alpha_{\text{eff}} = 0$).

(b) IID data, imperfect power control ($\alpha_{\text{eff}} = 2$).

(c) Non-IID data, ideal power control ($\alpha_{\text{eff}} = 0$).

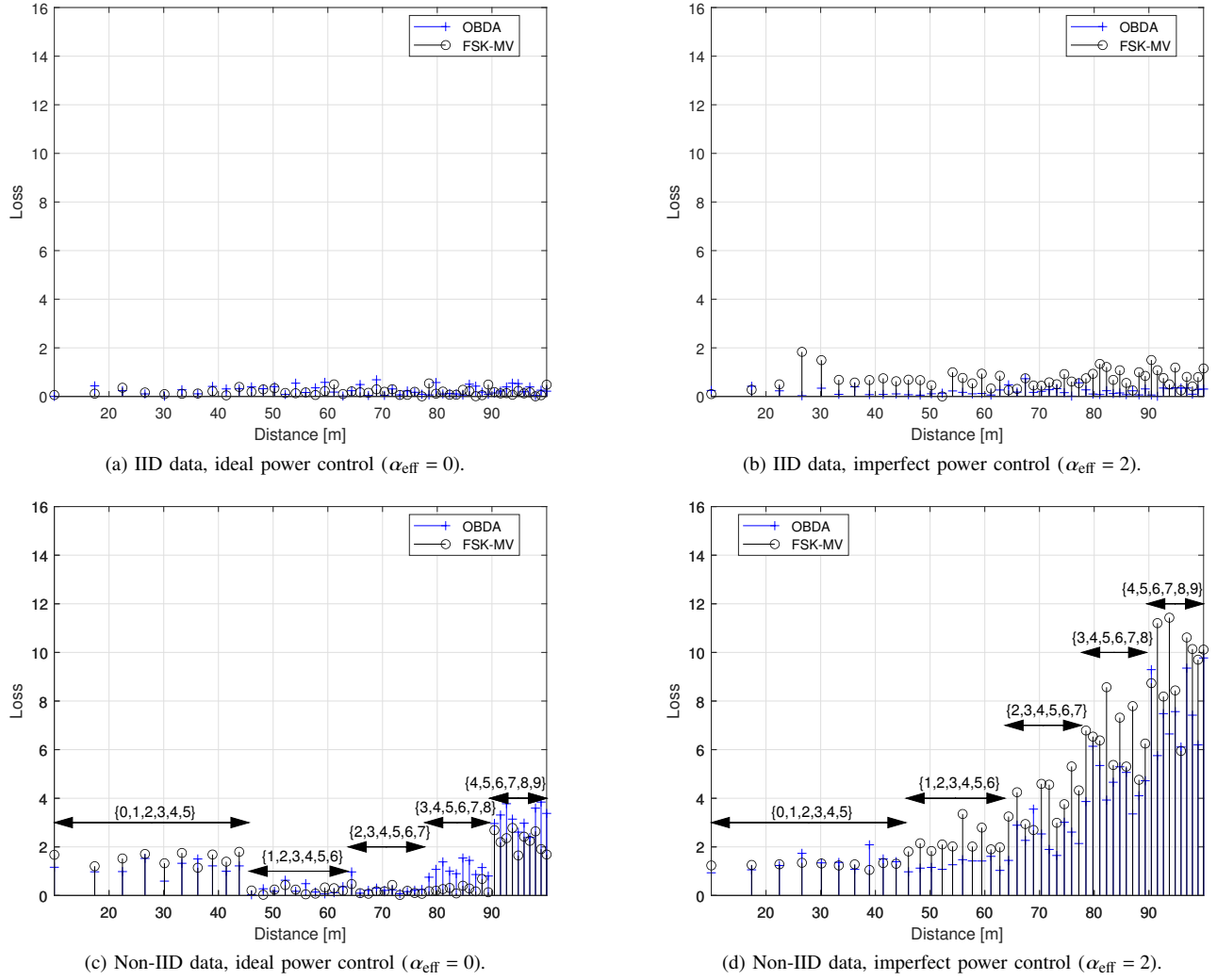(d) Non-IID data, imperfect power control ($\alpha_{\text{eff}} = 2$).

Fig. 5. Local loss versus link distance. For non-IID data, the data samples are function of the locations of EDs. Since the received signal power of the cell-edge EDs are dominated by the nearby EDs, only data samples at the nearby ED are learned. For this analysis, an ideal time synchronization is assumed in order to provide the results for OBDA. The available labels are indicated as $\{\cdots\}$.

described in [11]. Let $\mathbf{g}^{(n)}$ be the gradient of $F(\mathbf{w}^{(n)})$ (i.e., the true gradient). By using Assumption 2 and using (13), we can state that

$$F(\mathbf{w}^{(n+1)}) - F(\mathbf{w}^{(n)}) \leq -\eta \mathbf{g}^{(n)\mathrm{T}} \mathbf{v}^{(n)} + \frac{\eta^2}{2} \|\mathbf{L}\|_1$$

$$= -\eta \|\mathbf{g}^{(n)}\|_1 + \frac{\eta^2}{2} \|\mathbf{L}\|_1$$

$$+ 2\eta \sum_{i=1}^{q} |g_i^{(n)}| \mathbb{I}\left[\text{sign}\left(\Delta_i^{(n)}\right) \neq \text{sign}\left(g_i^{(n)}\right)\right] .$$

Therefore,

$$\mathbb{E}\left[F(\mathbf{w}^{(n+1)}) - F(\mathbf{w}^{(n)})|\mathbf{w}^{(n)}\right] \leq -\eta \|\mathbf{g}^{(n)}\|_1 + \frac{\eta^2}{2} \|\mathbf{L}\|_1$$

$$+ 2\eta \sum_{i=1}^{q} |g_i^{(n)}| \underbrace{\mathbb{P}\left[\text{sign}\left(\Delta_i^{(n)}\right) \neq \text{sign}\left(g_i^{(n)}\right)\right]}_{\triangleq P_i^{\text{err}}} .$$

$$\underbrace{\phantom{+ 2\eta \sum_{i=1}^{q} |g_i^{(n)}| \mathbb{P}\left[\text{sign}\left(\Delta_i^{(n)}\right) \neq \text{sign}\left(g_i^{(n)}\right)\right]}}_{\text{Stochasticity-induced error}}$$

The main challenge is to obtain an upper bound on the stochasticity-induced error. To address this, assume that $\text{sign}\left(g_i^{(n)}\right) = 1$. Let Z be a random variable for counting the number of EDs with the correct decision, i.e., $\text{sign}\left(g_i^{(n)}\right) = 1$. The random variable Z can then be model as the sum of K independent Bernoulli trials, i.e., a binomial variable with the success and failure probabilities given by

$$p_i \triangleq \mathbb{P}\left[\text{sign}\left(\tilde{g}_{k,i}^{(n)}\right) = \text{sign}\left(g_i^{(n)}\right)\right] ,$$

$$q_i \triangleq \mathbb{P}\left[\text{sign}\left(\tilde{g}_{k,i}^{(n)}\right) \neq \text{sign}\left(g_i^{(n)}\right)\right] ,$$

respectively, for all k. This implies that

$$P_i^{\text{err}} = \sum_{K_i^+=0}^{K} \mathbb{P}\left[\text{sign}\left(\Delta_i^{(n)}\right) \neq 1 | Z = K_i^+\right] \mathbb{P}\left[Z = K_i^+\right] ,$$

where $\mathbb{P}\left[Z = K_i^+\right] = \binom{K}{K_i^+} p_i^{K_i^+} q_i^{K-K_i^+}$. To calculate $\mathbb{P}\left[\text{sign}\left(\Delta_i^{(n)}\right) \neq 1 | Z = K_i^+\right]$, we use the distribution of
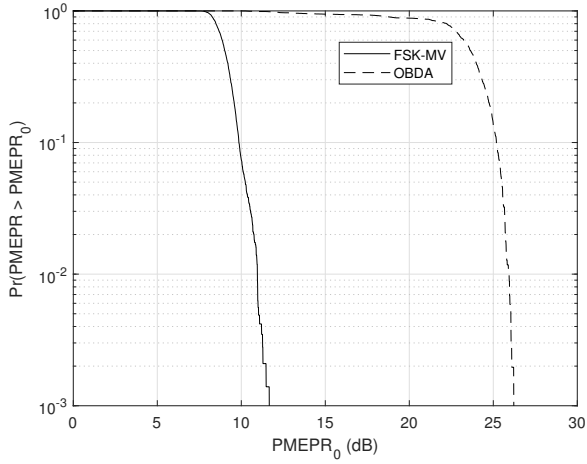
Fig. 6. PMEPR distributions. The randomization symbols in FSK-MV lowers PMEPR.

$\Delta_i^{(n)}$, which can be obtained by using the properties of exponential random variables as

$$f(\Delta_i^{(n)}) = \begin{cases} \dfrac{e^{-\frac{\Delta_i^{(n)}}{\mu_i^-}}}{\mu_i^+ + \mu_i^-}, & \Delta_i^{(n)} \leq 0 \\[2ex] \dfrac{e^{-\frac{\Delta_i^{(n)}}{\mu_i^+}}}{\mu_i^+ + \mu_i^-}, & \Delta_i^{(n)} > 0 \end{cases} . \tag{23}$$

Thus, by integrating (23) with respect to $\Delta_i^{(n)}$,

$$\mathbb{P}\left[\mathrm{sign}\left(\Delta_i^{(n)}\right) \neq 1 | Z = K_i^+\right] = \frac{\mu_i^-}{\mu_i^+ + \mu_i^-}$$
$$= \frac{(K - K_i^+) + 1/\xi}{K + 2/\xi}. \tag{24}$$

Hence, by using (24) and the properties of binomial coefficients

$$P_i^{\mathrm{err}} = \sum_{K_i^+=0}^{K} \frac{(K - K_i^+) + 1/\xi}{1 + 2/\xi} \binom{K}{K_i^+} p_i^{K_i^+} q_i^{K-K_i^+}$$
$$= \frac{\frac{1}{\xi K}}{1 + \frac{2}{K\xi}} + \frac{q_i}{1 + \frac{2}{\xi K}} . \tag{25}$$

Under Assumption 2 and Assumption 3, by using the derivations in [11], it can be shown that $q_i \leq \frac{\sqrt{2}\sigma_i}{3|g_i^{(n)}|\sqrt{n_b}}$. Hence, an upper bound on the stochasticity-induced error can be obtained as

$$\sum_{i=1}^{q} |g_i^{(n)}| P_i^{\mathrm{err}} \leq \frac{\frac{1}{\xi K}}{1 + \frac{2}{K\xi}} \|\mathbf{g}^{(n)}\|_1 + \frac{1}{\sqrt{n_b}} \frac{\sqrt{2}/3}{1 + \frac{2}{K\xi}} \|\boldsymbol{\sigma}\|_1 .$$

By rearranging the terms in (26) and using the expressions for n_b and η, (22) is reached. ∎

REFERENCES

[1] T. Gafni, N. Shlezinger, K. Cohen, Y. C. Eldar, and H. V. Poor, "Federated learning: A signal processing perspective," 2021. [Online]. Available: arXiv:2103.17150

Based on Assumption 1,

$$F(\mathbf{w}^{(0)}) - F^* \geq F(\mathbf{w}^{(0)}) - \mathbb{E}\left[F(\mathbf{w}^{(N)})\right]$$
$$= \mathbb{E}\left[\sum_{n=0}^{N-1} F(\mathbf{w}^{(n)}) - F(\mathbf{w}^{(n+1)})\right]$$
$$\geq \mathbb{E}\left[\sum_{n=0}^{N-1} \frac{\eta}{1 + \frac{2}{K\xi}} \|\mathbf{g}^{(n)}\|_1 - \frac{\eta^2}{2} \|\mathbf{L}\|_1 - \frac{\eta}{\sqrt{n_b}} \frac{2\sqrt{2}/3}{1 + \frac{2}{K\xi}} \|\boldsymbol{\sigma}\|_1\right] . \tag{26}$$

[2] M. Chen, D. Gündüz, K. Huang, W. Saad, M. Bennis, A. V. Feljan, and H. Vincent Poor, "Distributed learning in wireless networks: Recent progress and future challenges," *IEEE J. Sel. Areas Commun.*, pp. 1–26, 2021.

[3] H. Hellstrom, J. M. B. da Silva Jr, V. Fodor, and C. Fischione, "Wireless for machine learning," 2020.

[4] M. Goldenbaum, H. Boche, and S. Stańczak, "Harnessing interference for analog function computation in wireless sensor networks," *IEEE Trans. Signal Process.*, vol. 61, no. 20, pp. 4893–4906, Oct. 2013.

[5] W. Liu, X. Zang, Y. Li, and B. Vucetic, "Over-the-air computation systems: Optimization, analysis and scaling laws," *IEEE Trans. Wireless Commun.*, vol. 19, no. 8, pp. 5488–5502, Aug. 2020.

[6] B. Nazer and M. Gastpar, "Computation over multiple-access channels," *IEEE Trans. Inf. Theory*, vol. 53, no. 10, pp. 3498–3516, Oct. 2007.

[7] G. Zhu, Y. Wang, and K. Huang, "Broadband analog aggregation for low-latency federated edge learning," *IEEE Trans. Wireless Commun.*, vol. 19, no. 1, pp. 491–506, Jan. 2020.

[8] T. Sery, N. Shlezinger, K. Cohen, and Y. C. Eldar, "Over-the-air federated learning from heterogeneous data," 2020. [Online]. Available: arXiv:2009.12787

[9] M. M. Amiri and D. Gündüz, "Federated learning over wireless fading channels," *IEEE Trans. Wireless Commun.*, vol. 19, no. 5, pp. 3546–3557, Feb. 2020.

[10] G. Zhu, Y. Du, D. Gündüz, and K. Huang, "One-bit over-the-air aggregation for communication-efficient federated edge learning: Design and convergence analysis," *IEEE Trans. Wireless Commun.*, vol. 20, no. 3, pp. 2120–2135, Nov. 2021.

[11] J. Bernstein, Y.-X. Wang, K. Azizzadenesheli, and A. Anandkumar, "signSGD: Compressed optimisation for non-convex problems," in *Proc. in International Conference on Machine Learning*, vol. 80. Proceedings of Machine Learning Research, 10–15 Jul 2018, pp. 560–569.

[12] K. Yang, T. Jiang, Y. Shi, and Z. Ding, "Federated learning via over-the-air computation," *IEEE Trans. Wireless Commun.*, vol. 19, no. 3, pp. 2022–2035, 2020.

[13] M. M. Amiria, T. M. Duman, D. Gündüz, S. R. Kulkarni, and H. Vincent Poor, "Collaborative machine learning at the wireless edge with blind transmitters," *IEEE Trans. Wireless Commun.*, pp. 1–1, Mar 2021.

[14] E. Dahlman, S. Parkvall, and J. Skold, *5G NR: The Next Generation Wireless Access Technology*, 1st ed. USA: Academic Press, Inc., 2018.

[15] A. Şahin, B. Everette, and S. Hoque, "Over-the-air computation with DFT-spread OFDM for federated edge learning," in *Proc. IEEE Wireless Communications and Networking Conference (WCNC) (submitted)*, Apr. 2022, pp. 1–6.

[16] T. Zeng, O. Semiari, M. Mozaffari, M. Chen, W. Saad, and M. Bennis, "Federated learning in the sky: Joint power allocation and scheduling with UAV swarms," in *Proc. IEEE International Conference on Communications (ICC)*, 2020, pp. 1–6.

[17] Y. A. Jawhar, L. Audah, M. A. Taher, K. N. Ramli, N. S. M. Shah, M. Musa, and M. S. Ahmed, "A review of partial transmit sequence for PAPR reduction in the OFDM systems," *IEEE Access*, vol. 7, pp. 18 021–18 041, 2019.